IEEE Access
Multidisciplinary ⋮ Rapid Review ⋮ Open Access Journal

Received February 5, 2021, accepted February 15, 2021, date of publication February 22, 2021, date of current version March 4, 2021.

Digital Object Identifier 10.1109/ACCESS.2021.3061211

Single-Line-to-Ground Fault Location in Resonant Grounded Systems Based on Fault Distortions

YOUGEN CHEN, JUNBO YIN, ZHIYONG LI, AND RENYONG WEI
School of Automation, Central South University, Changsha 410083, China

Corresponding author: Zhiyong Li (lizy@mail.csu.edu.cn)

This work was supported by the Graduate Innovation Program of Central South University under Grant GCX2020333Y.

ABSTRACT Under single-line-to-ground (SLG) faults, the voltages and currents in resonant grounded systems will inevitably be distorted. To locate the faults quickly and accurately, this paper proposes a location method based on fault distortions. The faulty phase is firstly detected according to the first SLG fault feature below, and then the faulty feeder and section are detected according to the second feature below. 1) On the bus, one of the following distortions occurs. One dropped faulty-phase voltage (FPV) and two raised normal-phase voltages (NPVs). One dropped FPV and two NPVs (in which one rises and the other drops), where the product of FPV amplitude distortion and its phase-angle distortion is unique among three phase voltages. 2) On the faulty phase, the current on faulty feeder upstream rises, while the currents on faulty feeder downstream and normal feeders drop. Compared to existing methods, simulation tests show that the proposed method is robust under high impedance faults, and has a simple algorithm and easy engineering implementation. Also, it is effective under harmonics, three-phase imbalance, and different fault positions.

INDEX TERMS Fault distortions, fault location, single-line-to-ground faults, resonant grounded systems.

ACRONYMS

SLG	Single line to ground
(F/N) PV	(Faulty/Normal) phase voltage
RGS	Resonant grounded system
ZSC	Zero-sequence current
FF (U/D)	Faulty feeder (upstream/downstream)
FPC	Faulty phase current
VFA	Voltage fault area: K_u
FD	Fault distortion: Δ
Z_f / Y_f	Fault impedance/admittance
$I_{u/d/n}$	FPC on FFU/FFD/normal-feeder
$E_{a/b/c}$	Pre-fault bus voltages
$U_{fa/nb/nc}$	Post-fault bus voltages
$\Delta_{\theta/U/I}$	Phase-angle/Voltage/Current FD
Y_{eq}	Total equivalent admittance on bus
$Y_{eq(n)}$	Equivalent admittance on faulty $Feeder_{(n)}$
$Y_{eq(j)}$	Equivalent admittance on normal $Feeder_{(j)}$
Y_p	Admittance of Peterson coil

I. INTRODUCTION

SLG faults are the fault type with the highest incidence in distribution networks, accounting for more than 80% [1]. To ensure user safety and power supply reliability, the 6-66 kV distribution networks in China mainly use the resonant grounded system (RGS). The advantages of RGS include small fault currents, symmetrical line voltages, and loads that can continue to run for 1-2 hours. However, the FPV is close to 0 and NPVs are close to line voltages under low impedance faults. If the system runs with the faults for a long time, it will not only threaten personal and equipment safety, but also lead to more serious phase-to-phase short circuit faults. Therefore, SLG faults must be located and removed in a short time.

At present, SLG fault detection problems have not been well solved. Many distribution departments in China still use the traditional ''pull-feeder'' method, which detects the faulty feeder by disconnecting feeders in turn and observing whether the fault indication signal disappears. This traditional method not only causes unnecessary power loss to users, but also is not conducive to personal and equipment safety, and cannot further locate the faults.

A. PREVIOUS AND RELATED WORKS

In recent years, researchers have proposed many fault detection methods suitable for their distribution networks.

In [2], the Peterson coil was adjusted after faults to make the zero-sequence current (ZSC) on faulty feeder

The associate editor coordinating the review of this manuscript and approving it for publication was Dazhong Ma.

upstream (FFU) exceed a threshold, so as to locate the faults. In [3], a method based on instantaneous ZSC energy was proposed, which detects the faulty feeder according to the feature of maximum instantaneous ZSC energy in the selected frequency band on the faulty feeder. In [4], the average data distribution deviation of instantaneous ZSC was used to detect the faulty feeder. In [5], the relationship between the initial transient ZSC and FPV was used to detect the faulty feeder. In [6], a method based on grey correlation was proposed to detect faults by comparing the similarity on transient ZSC waveforms of faulty and normal feeders. In [7], the faulty feeder was detected by comparing ZSC directions of faulty and normal feeders.

In [8], the improved empirical wavelet transform was used to extract the natural mode function of original signal, and then the fault probability of each feeder was estimated. In [9], the fuzzy c-means algorithm was used to determine the fault and non-fault states of feeders, and then the faulty feeder was detected by the distance between fault state feature samples and cluster centers. In [10], a method based on the continuous wavelet transform and convolution neural network was proposed to detect faulty feeders. In [11], the S-transform and continuous wavelet transform were used to locate faults on the combination of overhead feeders and cables. In [12] and [13], the Hilbert-Huang transform was used to extract instantaneous power directions of each feeder, so as to detect high impedance faults. In [14] and [15], the mathematical morphology was proposed to process continuous signals in the nonlinear time domain, and the improved mathematical morphology algorithm was used to identify distribution network faults [16].

In [17], according to the feature that the reactive current in faulty feeders was larger than that in normal feeders, the faulty feeder was detected. In [18], the faulty feeder was detected by traveling wave polarities of the post-fault current and voltage. In [19], new generation mechanisms of the zero-sequence voltage and residual current were proposed, and the faulty feeder was detected by an improved zero-sequence admittance method. In [20], a method based on the correlation dimension and average resistance was proposed to identify the cause of permanent SLG faults.

In [21], a data-driven fault location method for distributed generation and distribution systems was proposed, in which the fault reports of smart meters were used to predict the fault section. In [22], a fault location method based on fault indicators was proposed, in which the relationship matrix between fault location systems and fault control systems was used. In [23], the relationship between fault distances and cluster measurement groups was used to locate the fault section. In [24], the synchronized distributed voltage traveling wave observers were used to locate faults, and the effect of power system components on traveling wave propagations was studied.

However, many of the above methods have not been widely used in practice. The main reasons are as follows.

1) Under high impedance faults, the ZSC is quite small and difficult to extract, which leads to the failure on some ZSC-based methods such as [2] and [3].
2) Some smart methods, such as [8] and [9], focus on the signal transformation and processing, and their algorithms are complex and difficult to implement in engineering.
3) Some methods, such as [17] and [18], can only detect faulty feeders, but cannot further locate faults. The improvement to manual troubleshooting efficiency and reduction to power outage time are limited.
4) Some methods, such as [21] and [22], require the smart devices such as smart meters, fault location systems, and fault control systems. They are only applicable to some economically developed countries.

B. CONTRIBUTIONS

Aiming at the above problems, the innovations of this paper are as follows.

1) The SLG fault features of bus voltages and faulty phase currents (FPCs) on feeders are obtained:
   - There are three types of bus voltage distortions. One dropped FPV and two raised NPVs. One dropped FPV and two NPVs (in which one rises and the other drops), where the product of FPV amplitude distortion and its phase-angle distortion is unique among three phase voltages.
   - The FPC on FFU rises, while the FPCs on faulty feeder downstream (FFD) and normal feeders drop.
2) The voltage fault area (VFA) and fault distortion (FD) are defined to quantify the distortion degrees of above voltages and currents. Also, a fault location method based on FDs is proposed, including faulty phase and feeder detections.
3) The proposed method only needs the pre-fault and post-fault bus voltages and feeder FPCs extracted by common low-cost current transformers, and its algorithm is simple. Their values are easy to extract even under high impedance faults.

The rest of this paper is organized as follows. Section II analyzes the steady-state SLG fault features in RGS, including bus voltages and feeder FPCs. Section III proposes a fault location method based on FDs and introduces its engineering implementation. Aiming at the fault features and proposed method, Section IV conducts simulation verifications and tests, including comparisons with existing methods. iConclusions are drawn in Section V. Appendix contains the derivation for some equations.

II. SLG FAULT FEATURES IN RGS

For Fig. 1, it is assumed that the bus voltages $E_{a/b/c}$ and line parameters are symmetrical, and the capacitances between phases are ignored. The system neutral is grounded by the Peterson coil Z_p. $Z_{eq(1)} - Z_{eq(n)}$ are equivalent impedances

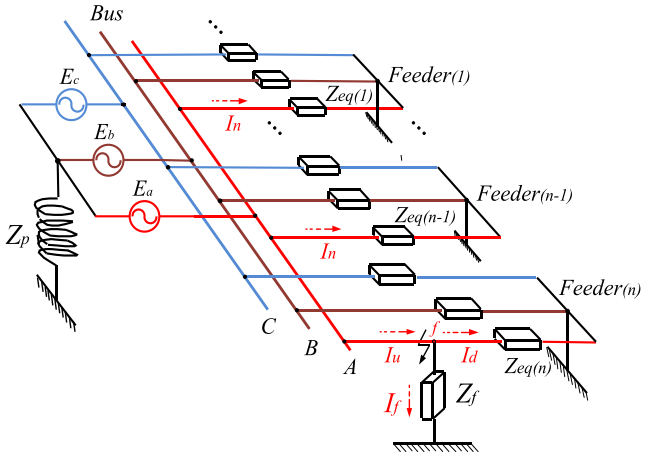

FIGURE 1. Steady-state model of RGS under SLG faults.

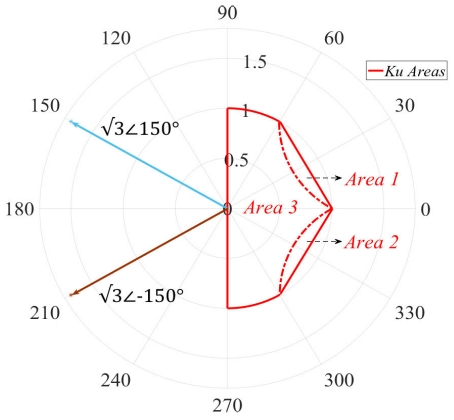

FIGURE 2. Polar diagrams for K_u and $\sqrt{3}\angle \pm 150°$.

from the bus to loads on $Feeder_{(1)} - Feeder_{(n)}$:

$$Z_{eq(n)} = Z_{l(n)} + Z_{t(n)} + Z_{load(n)} \tag{1}$$

where $Z_{l(n)}$, $Z_{t(n)}$, and $Z_{load(n)}$ are the line, transformer, and load impedances.

When a SLG fault occurs at the phase A on $Feeder_{(n)}$ and the system enters into a steady state, it is equivalent to connecting a fault impedance Z_f in parallel with the phase A. In Fig. 1, I_u and I_d are the FPCs on FFU and FFD, and I_n is the FPCs on normal feeders. I_f is the fault current:

$$I_f = \frac{3E_a}{3Z_f + Z_1 + Z_2 + Z_0} \tag{2}$$

where Z_1, Z_2, and Z_0 are the Thevenin impedances in positive, negative, and zero-sequence networks [25].

A. BUS VOLTAGES

The feeders in distribution networks are generally no more than 100 km. When the working frequency is stable at 50/60 Hz, the impedance on FFU is far less than that on FFD containing loads. Therefore, the bus and fault point can be considered as same potential when studying bus voltages.

The post-fault FPV on the bus is

$$U_{fa} = Z_f I_f = \frac{3Z_f}{3Z_f + Z_1 + Z_2 + Z_0} E_a = K_u E_a \tag{3}$$

where K_u is defined as the VFA. Its amplitude $|K_u| < 1$ indicates that the FPV drops under SLG faults, and it is directly proportional to Z_f: the smaller Z_f, the lower FPV. Also, the phase angle of K_u satisfies $\theta_{Ku} \in [-90°, 90°]$.

The post-fault NPVs on the bus are

$$U_{nb} = E_b - E_a + U_{fa} = (K_u + \sqrt{3}\angle -150°)E_a \tag{4}$$

$$U_{nc} = E_c - E_a + U_{fa} = (K_u + \sqrt{3}\angle 150°)E_a \tag{5}$$

where E_a, E_b, and E_c are pre-fault bus voltages. Equations (3)-(5) show that under SLG faults, the amplitude and phase angle of bus voltages will suddenly change (i.e., distortion).

The K_u and $\sqrt{3}\angle \pm 150°$ are shown in Fig. 2, where K_u can be divided into Area 1-3. According to (3)-(5), U_{fa}/E_a, U_{nb}/E_a, and U_{nc}/E_a are shown in Fig. 3 when K_u is in Area 1-3.

Fig. 3 shows that when K_u is in the different Areas, U_{fa}, U_{nb}, and U_{nc} show different features under SLG faults. For example, in Fig. 3(a) (K_u in Area 1), $\left|U_{fa}/E_a\right| < 1$ and $\theta_{(U_{fa}/E_a)} \in [0, 60°]$ show that the amplitude of FPV-A drops and its phase angle increases $[0, 60°]$. Also, $|U_{nb}/E_a| < 1$ and $\theta_{(U_{nb}/E_a)} \in [-180°, -120°]$ show that the amplitude of NPV-B drops and its phase angle decreases $[0, 60°]$. Also, $|U_{nc}/E_a| > 1$ and $\theta_{(U_{nc}/E_a)} \in [120°, 125.26°]$ show that the amplitude of NPV-C rises and its phase angle increases $[0, 5.26°]$.

Similarly, when K_u is in Area 2 or 3, the distortion features on bus voltages can be obtained, as shown in Table 1. In this paper, Δ in the table is defined as the FD, which represents the difference between the pre-fault and post-fault parameters. For example, Δ_U and Δ_θ are the voltage FD and phase angle FD, which are determined by (6) and (7).

$$\Delta_\theta = \theta' - \theta \tag{6}$$

where θ and θ' are the pre-fault and post-fault phase angles on bus voltages. If Δ_θ is positive (or negative), it means that the phase angle increases (or decreases) under SLG faults.

$$\Delta_U = \left|U'\right| - |U| \tag{7}$$

where $|U|$ and $\left|U'\right|$ are the pre-fault and post-fault amplitudes on bus voltages. If Δ_U is positive (or negative), it means that the amplitude rises (or drops) under SLG faults.

Table 1 shows that there are three types of bus voltage distortions under SLG faults, depending on K_u, which is composed of system parameters and fault impedances.

In summary, the FPV will inevitably drop. For two NPVs, there are one rise and one drop, or there are two rises.

B. FPCs ON FEEDERS

To facilitate calculations, we combine feeders on the same phase in Fig. 1, and replace impedances Z with

TABLE 1. Distortions of voltage amplitude and phase angle with K_u under SLG faults.

K_u	*Faulty phase A*		*Normal phase B*		*Normal phase C*	
	Δ_{Ua} (V)	$\Delta_{\theta a}$ (°)	Δ_{Ub} (V)	$\Delta_{\theta b}$ (°)	Δ_{Uc} (V)	$\Delta_{\theta c}$ (°)
Area 1	-	0 to 60	-	-60 to 0	+	0 to 5.26
Area 2	-	-60 to 0	+	-5.26 to 0	-	0 to 60
Area 3	-	-90 to 90	+	-65.26 to 0	+	0 to 65.26

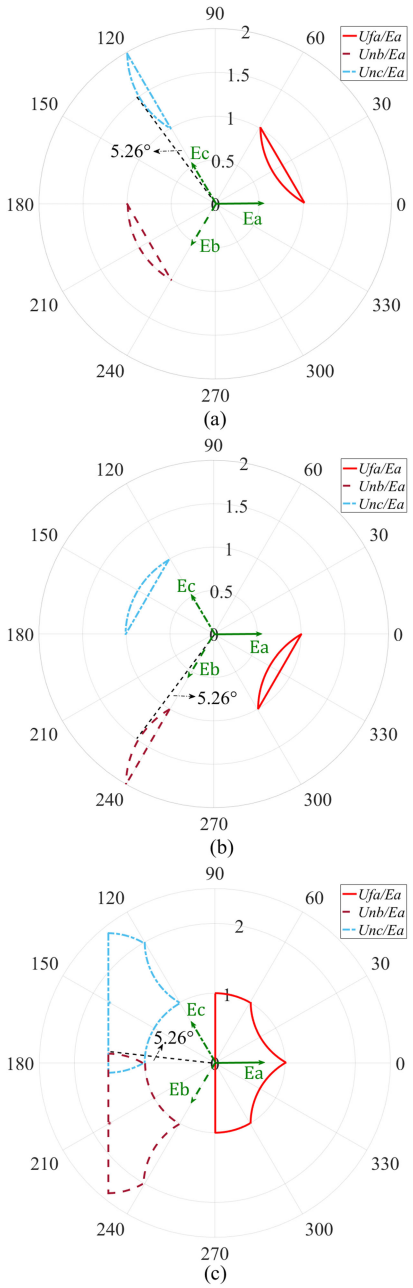

FIGURE 3. Distortions of U_{fa}, U_{nb}, and U_{nc} with K_u. (a) K_u in Area 1. (b) K_u in Area 2. (c) K_u in Area 3.

admittances Y. Then, we can get the equivalent fault model shown in Fig. 4, where Y_{eq} is

$$Y_{eq} = \sum_{i=1}^{n} Y_{eq(i)} \tag{8}$$

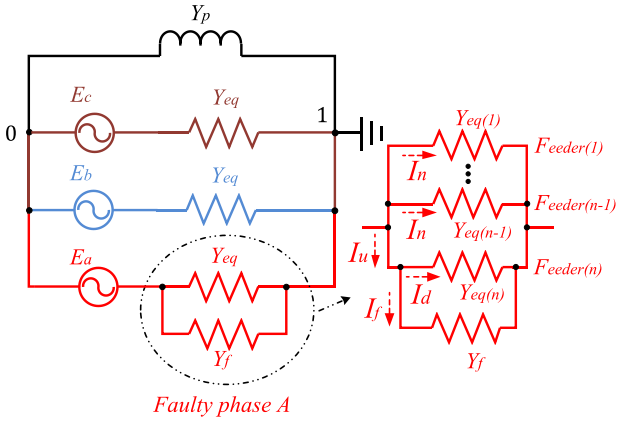

FIGURE 4. Equivalent model of RGS under SLG faults.

To quantify the current distortion under SLG faults, the current FD Δ_I is introduced as

$$\Delta_I = \left|I'\right| - |I| \tag{9}$$

where $|I|$ and $\left|I'\right|$ are the pre-fault and post-fault current amplitudes on the same feeder of same phase.

1) FPC ON FFU

The pre-fault system is symmetric, so the pre-fault FPC on FFU is $Y_{eq(n)}E_a$.

By establishing the Nodal Admittance Equation for Fig. 4 (see Appendix), the post-fault FPC on FFU can be obtained as

$$I_u = \frac{3Y_{eq} + Y_p}{3Y_{eq} + Y_p + Y_f}\left(Y_{eq(n)} + Y_f\right)E_a \tag{10}$$

Therefore, the Δ_I of FPC on FFU is

$$\Delta_{Iu} = |I_u| - \left|Y_{eq(n)}E_a\right| > 0 \tag{11}$$

Equations (10)-(11) show that the FPC on FFU rises under SLG faults, and the raised amplitude is proportional to fault admittances Y_f. In other words, it is inversely proportional to Z_f.

2) FPC ON FFD

Before faults, the FPC on FFD is the same as FPC on FFU, and it is $Y_{eq(n)}E_a$.

The post-fault FPC on FFD is

$$I_d = \frac{3Y_{eq} + Y_p}{3Y_{eq} + Y_p + Y_f}Y_{eq(n)}E_a \tag{12}$$

TABLE 2. FDs of FPCs on feeders.

FDs	*FFU*	*FFD*	*Normal feeders*
Δ_I (A)	+	-	-

Therefore, the Δ_I of FPC on FFD is

$$\Delta_{Id} = |I_d| - \left|Y_{eq(n)}E_a\right| < 0 \tag{13}$$

Equations (12)-(13) show that the FPC on FFD drops under SLG faults, and the dropped amplitude is proportional to Y_f.

3) FPCs ON NORMAL FEEDERS

Before faults, the FPCs on normal feeders are $Y_{eq(j)}E_a$, where $j = 1, 2, \cdots, n-1$.

The post-fault FPCs on normal feeders are

$$I_n = \frac{3Y_{eq} + Y_p}{3Y_{eq} + Y_p + Y_f} Y_{eq(j)}E_a \tag{14}$$

Therefore, the Δ_I of FPCs on normal feeders are

$$\Delta_{In} = |I_n| - \left|Y_{eq(j)}E_a\right| < 0 \tag{15}$$

Equations (14)-(15) show that the FPCs on normal feeders drop under SLG faults, and the dropped amplitude is proportional to Y_f.

In summary, the FDs of FPCs on feeders are shown in Table 2.

III. FAULT LOCATION METHOD BASED ON FDs

From Section II, we can see that the RGS under SLG faults will present: 1) The bus voltages are distorted according to Table 1; 2) The FPCs on feeders are distorted according to Table 2. Therefore, this Section will design a fault location method according to the above features, and describe its engineering implementation.

A. FAULTY PHASE DETECTION

Under SLG faults, there are one dropped FPV and two raised NPVs when K_u is in Area 3. In other words, the only dropped-voltage phase on the bus is the faulty phase.

When K_u is in Area 1 or 2, there are one dropped FPV and two NPVs in which one rises and the other drops. At this time, $\Delta_U \cdot \Delta_\theta$ on each voltage are shown in Table 3. Table 3 shows that there are $\Delta_U \cdot \Delta_\theta < 0$ for FPV and $\Delta_U \cdot \Delta_\theta > 0$ for NPVs when K_u is in Area 1; there are $\Delta_U \cdot \Delta_\theta > 0$ for FPV and $\Delta_U \cdot \Delta_\theta < 0$ for NPVs when K_u is in Area 2. In other words, whether K_u is in Area 1 or 2, the $\Delta_U \cdot \Delta_\theta$ of FPV is unique among the three phase voltages. Therefore, the phase with unique $\Delta_U \cdot \Delta_\theta$ on the bus can be determined as the faulty phase.

In summary, after SLG faults occur, the pre-fault and post-fault bus voltages can be extracted to calculate the voltage FDs (Δ_U) according to (7). If there is only one phase with $\Delta_U < 0$, this phase is determined as the faulty phase. Otherwise, the products $\Delta_U \cdot \Delta_\theta$ on each phase are further calculated to determine that the phase with unique $\Delta_U \cdot \Delta_\theta$ is the faulty phase.

TABLE 3. Products of voltage FDs and phase angle FDs.

K_u	*Faulty phase A*	*Normal phase B*	*Normal phase C*
	$\Delta_{Ua} \cdot \Delta_{\theta a}$	$\Delta_{Ub} \cdot \Delta_{\theta b}$	$\Delta_{Uc} \cdot \Delta_{\theta c}$
Area 1	-	+	+
Area 2	+	-	-

B. FAULTY FEEDER AND SECTION DETECTIONS

Table 2 shows that under SLG faults, the FPC on FFU rises and FPCs on normal feeders drop. Therefore, after the faulty phase detection, the pre-fault and post-fault FPCs on feeders can be extracted to obtain the current FDs (Δ_I) according to (9). Then it is determined that the feeder with $\Delta_I > 0$ is the faulty feeder, and the feeders with $\Delta_I < 0$ are the normal feeders.

After the above detections, the faulty phase and feeder have been determined. However, for long-term or permanent faults, Automatic Reclosing cannot make the system return to normal, only manual inspection and troubleshooting along the feeder. If the faulty section can be further detected, the labor efficiency can be improved and the power outage loss can be greatly reduced.

Table 2 shows that on the faulty feeder of faulty phase, there are $\Delta_I > 0$ for FFU and $\Delta_I < 0$ for FFD. Therefore, the pre-fault and post-fault FPCs at current transformers (CTs) on the faulty feeder can be extracted to obtain the Δ_I. If there are $\Delta_I > 0$ for CT_i and $\Delta_I < 0$ for CT_{i+1}, the fault is located in [CT_i, CT_{i+1}] (i.e., faulty section).

C. METHOD ENGINEERING IMPLEMENTATION

According to Section III.A-B, the FDs-based fault location method shown in Fig. 5 includes 3 steps: 1) faulty phase detection; 2) faulty feeder detection; 3) faulty section detection. Also, its start is determined by the zero-sequence voltage U_0 on the bus: $U_0 > U_{th}$; where U_{th} is usually (3-10) % of rated voltages [3].

In Step 1, in addition to the direct bus extraction, the voltages can also be extracted by any feeder connected to the bus. The distribution networks are usually equipped with bus monitoring devices. Step 2 requires the FPCs on feeders, so only one CT is installed at each feeder, and it can also identify bus faults. Step 3 requires the distributed CTs on the faulty feeder. Similar to phase measurement units (PMUs) [26], the low-cost distributed CTs may become another important component of smart grids. The number and spacing of distributed CTs can be defined by users according to fault experiences, which is flexible.

For the pre-fault and post-fault data capacities, to ensure accurate sampling and less calculations, it is only necessary to take respectively two-cycle (Close to fault cycle) average values excluding the transient process.

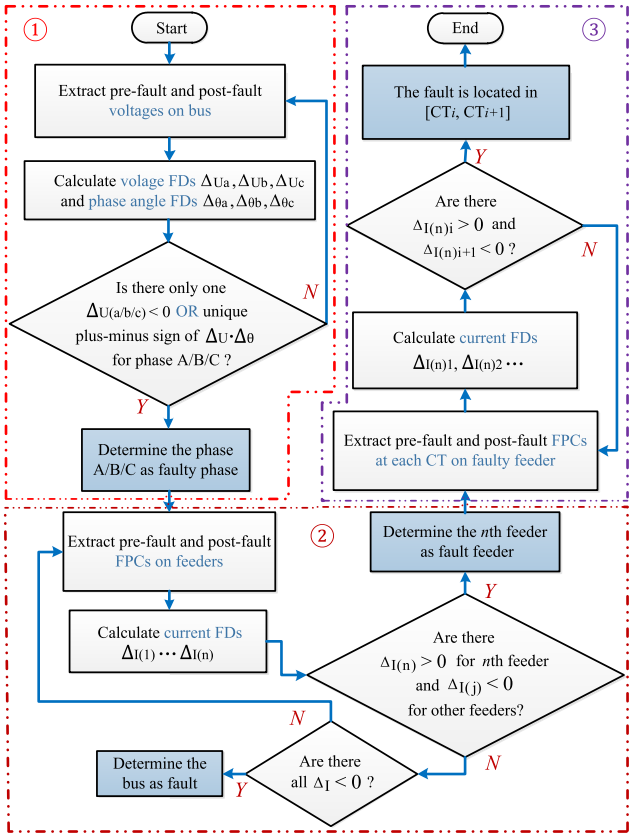

FIGURE 5. Fault location method based on FDs.

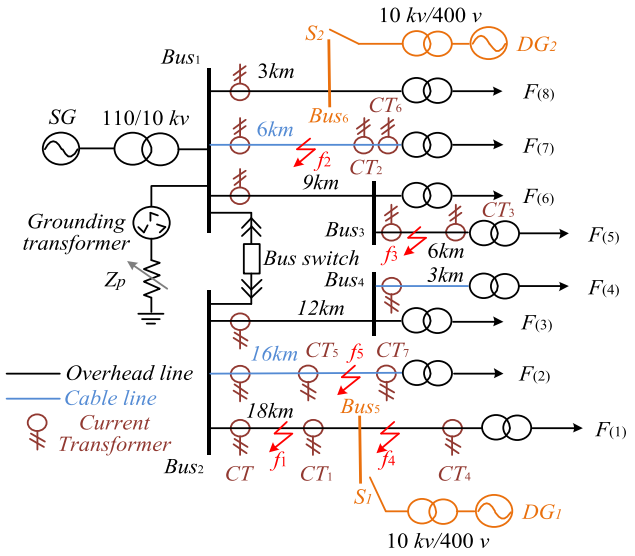

FIGURE 6. RGS simulation model under SLG faults.

In fact, CTs will inevitably have measurement errors, but the core of this method is to calculate the difference Δ between the pre-fault and post-fault. The error on the same CT exists before and after faults, and its impact has been automatically eliminated in the calculation according to (6), (7), and (9).

For the normal voltage and current fluctuation caused by factors such as parallel connection of capacitor groups, if it occurs before this method starts, its impact can also be automatically eliminated. If it occurs when this method is running (the probability is quite small, because the execution time of this method is at the MS level, see Section IV.D), its impact can be eliminated by adding low-pass filters or taking the average on multiple samples.

In particular, this method is based on steady-state fault features, so the transient factors such as transient high frequencies have no effect on this method. In engineering, (3-5) τ is considered as transient duration, where τ is the system time constant and determined by system parameters [27].

IV. SIMULATION VERIFICATIONS AND TESTS

Combined with actual distribution networks, we comprehensively consider the combined overhead and cable feeders $F_{(1)} - F_{(8)}$, and build the model shown in Fig. 6 by *Simulink*. The feeder parameters are shown in Table 4 [28]. In the figure, the 110 kV source generator (SG) and 400 V distributed generations (DG_1 and DG_2) are programmable three-phase voltage sources with RL branch, which can generate harmonics and three-phase imbalance. The loads are the three-phase parallel RLC with a rated voltage of 400 V. $f_1 - f_5$ are fault positions of 1, 3, 5, 8, and 15 km from the bus, and CTs are installed at each feeder. SLG faults occurred at Time = 200 ms. Also, in Section IV.A-C, the switches S_1 and S_2 are open to simulate single-source radial networks; in Section IV.D, the S_1 and S_2 are closed to simulate distributed networks with DGs.

A. TESTS FOR BUS VOLTAGES

Under the ideal condition without harmonics, there are at most three types of bus voltage distortions when the phase A is grounded by different Z_f and positions. They are shown in Fig. 7, where the pre-fault bus voltage amplitudes are 6643 V. The phase angles corresponding to Fig. 7(a) and (b) are shown in Fig. 8(a) and (b), where the pre-fault bus voltage phase angles are unified to $-3°$. The results show:

1) When Z_f is low, the transient overvoltage as shown in Fig. 7(c) will appear at the fault time, and the transient time lasts for about one cycle, accompanied by decaying oscillations (see Fig. 8). The amplitude and phase angle of bus voltages have significant changes (distortions) under SLG faults.
2) In Fig. 7(a), the voltages of phase A and B drop, while the voltage of phase C rises. It can be seen from Table 1 that K_u is in Area 1. In Fig. 7(b), the voltages of phase A and C drop, and the voltage of phase B rises; K_u is in Area 2. In Fig. 7(c), the voltage of phase A drops, and the voltages of phase B and C rise; K_u is in Area 3. Therefore, there are three types of bus voltage distortions under faults. One dropped FPV and two raised NPVs; one dropped FPV and two NPVs in which one

TABLE 4. Simulation parameters.

Feeder type	*Resistance* (Ω/km)		*Inductance* (mH/km)		*Capacitance* (uF/km)	
	Positive sequence	Zero sequence	Positive sequence	Zero sequence	Positive sequence	Zero sequence
Overhead feeder	0.170	0.320	1.017	3.560	0.115	0.006
Cable	0.270	2.700	0.255	1.109	0.376	0.276

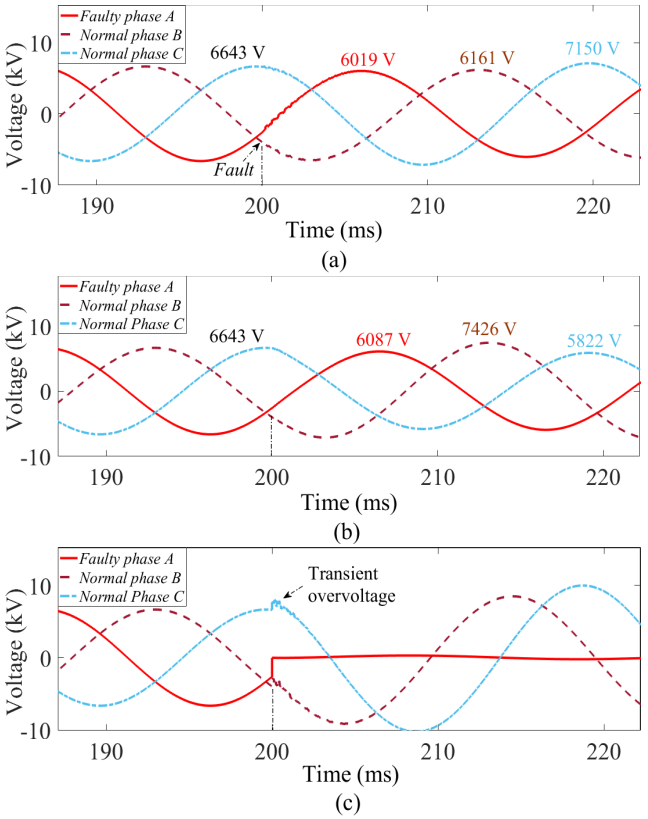

FIGURE 7. Bus voltages under different ku areas. (a) Area 1. (b) Area 2. (c) Area 3.

rises and the other drops. They are consistent with the voltage amplitude features described in Section II.A.

3) In Fig. 8(a), the phase angle of phase A increases by 6.29°, phase B decreases by 9.22°, and phase C increases by 3.54° under faults. In Fig. 8(b), the phase A decreases by 1.83°, phase B decreases by 4.95°, and phase C increases by 6.44°. Therefore, there are $\Delta_{\theta a} > 0, \Delta_{\theta b} < 0, \Delta_{\theta c} > 0$ when K_u is in Area 1, and there are $\Delta_{\theta a} < 0, \Delta_{\theta b} < 0, \Delta_{\theta c} > 0$ when K_u is in Area 2. They are consistent with the voltage phase angle features described in Section II.A.

In actual distribution networks, there are harmonics generated by non-linear loads such as power converters, and we can simulate the harmonics by the programmable SG. The bus voltages are shown in Fig. 9 (a)-(c) when the phase A is grounded by 10-2000 Ω at $f_1 - f_4$. Also, Under the case of 10 Ω, the Fast Fourier Transform (FFT) to FPV-A is shown in Fig. 9(d). The pre-fault bus voltage amplitudes are 6556 V. The results show:

1) All FPVs drop in Fig. 9(a), while all NPVs rise in Fig. 9(b) and (c), indicating that K_u is in Area 3 under the four fault cases.
2) In Fig. 9(a), even if Z_f is 2000 Ω (high impedance fault), the post-fault FPV is 6539 V, and still lower than the pre-fault. Also, with decreases of Z_f, the FPV is lower, which is consistent with (3).
3) In Fig. 9(b) and (c), even if Z_f is 2000 Ω, the post-fault NPVs are 6564 and 6562 V, they are still higher than the pre-fault. Also, in Fig. 9(d), the total harmonic distortion (THD) of FPV-A reaches 8.2%, which has exceeded the limit (the THD limit in China's distribution networks is 8%). They show that the harmonics, fault impedances, and fault positions do not change the fault features.

B. TESTS FOR FPCs ON FEEDERS

Under the ideal condition, the FPCs on feeders are shown in Fig. 10 when f_2 is grounded by 0.1 Ω. The faulty feeder includes FFU and FFD, and the pre-fault and post-fault current amplitudes on some feeders have been marked.

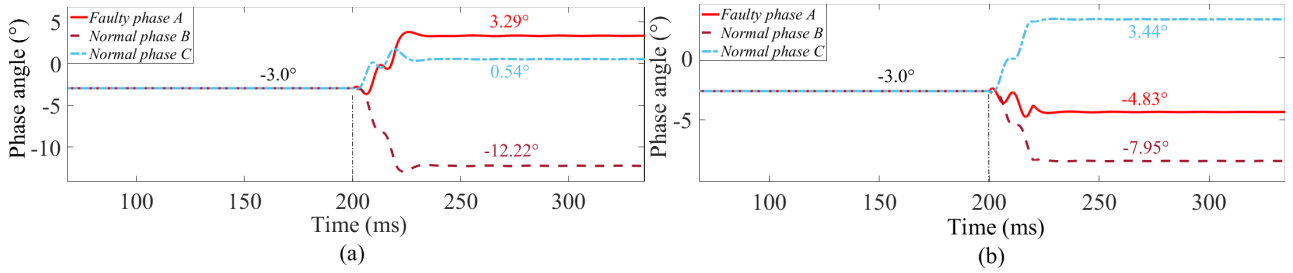

FIGURE 8. Bus voltage phase angles under different ku areas. (a) Area 1. (b) Area 2.

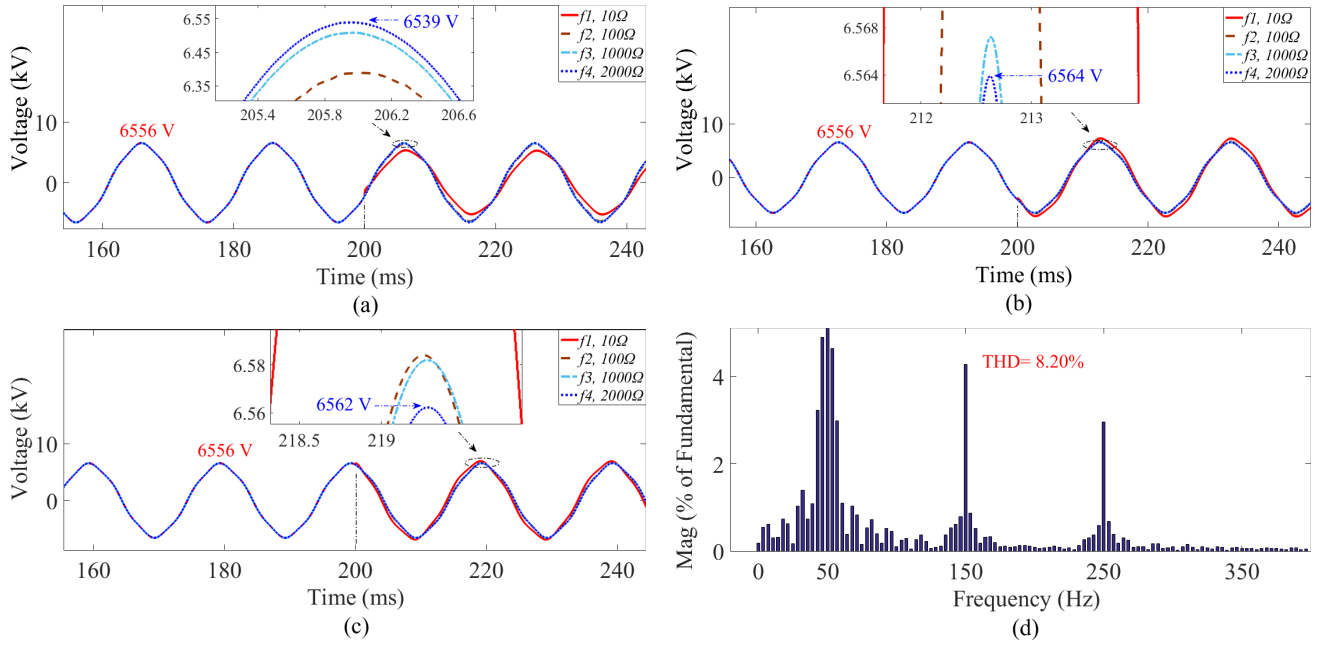

FIGURE 9. Bus voltages under different fault cases. (a) Faulty phase A. (b) Normal phase B. (c) Normal phase C. (d) FFT to FPV-A.

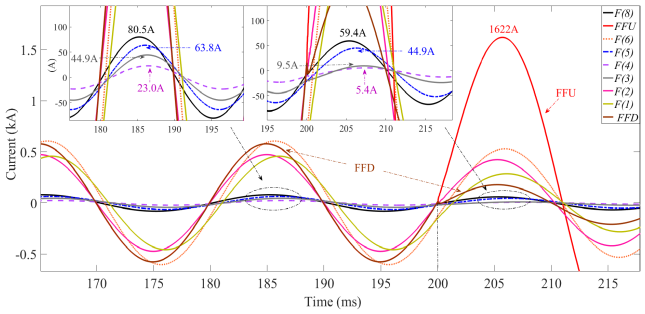

FIGURE 10. FPCs on each feeder when Z_f is 0.1 Ω.

In Fig. 10, the different equivalent impedances on feeders lead to the different FPCs. The post-fault FPC on FFU reaches 1622 A, which is significantly higher than the pre-fault. On the contrary, the FPCs on FFD and normal feeders drop. For example, the pre-fault and post-fault FPCs on the normal feeder $F_{(8)}$ are 80.5 and 59.4 A. They are consistent with the FPC features described in Section II.B.

Under harmonics, the FPCs on feeders are shown in Fig. 11(a)-(c) when the phase A is grounded by 10-2000 Ω at $f_1 - f_4$, and $F_{(2)}$ is taken as an example of normal feeders. Also, Under the case of 10 Ω, the FFT to FPC-on-FFD is shown in Fig. 11(d). The results show:

1) Since f_1 and f_4 are both fault positions on $F_{(1)}$, the pre-fault FPCs on faulty feeder under the two cases are the same (they coincide in the figure). The FPCs are both 447.9 A in Fig. 11(a), and are both 448.9A in Fig. 11(b).
2) In Fig. 11(a), the FPCs on FFU rise under faults. For example, the pre-fault and post-fault FPCs are 595.7 and 612.6 A when Z_f is 1000 Ω; the pre-fault and post-fault FPCs are 447.9 and 454.1A when Z_f is 2000 Ω. It is consistent with the FFU feature described in Section II.B.
3) In Fig. 11(b), the FPCs on FFD drop under faults. For example, the pre-fault and post-fault FPCs are 596.2 and 586.2 A when Z_f is 1000 Ω; the pre-fault and post-fault FPCs are 448.9 and 446.5 A when Z_f is 2000 Ω. It is consistent with the FFD feature described in Section II.B.
4) In Fig. 11(c), the pre-fault FPC on normal feeder $F_{(2)}$ is 460.3 A, and its FPC drops regardless of fault impedances and positions. For example, the FPC drops to 459.8 A when Z_f is 2000 Ω; with decreases of Z_f, the FPC is lower. It is consistent with the normal feeder feature described in Section II.B.
5) In Fig. 11(d), the THD reaches 6.49%, which is close to the limit. They show that the harmonics, fault impedances, and fault positions do not change the distortion features of FPCs: FFU rises, FFD and normal feeders drop. Also, the distortion degree become more serious with decreases of Z_f.

C. TESTS FOR PROPOSED METHOD

Under harmonics, the results of faulty phase, feeder, and section detections are shown in Tables 5, 6, and 7 with comprehensive consideration of different Z_f and fault positions. The faulty phases are all set to A.

Table 5 shows the Δ_U, Δ_θ, and faulty phase detection results under 5 cases, where \ means that this value does not need to be measured or calculated. Also, the fault currents corresponding to Case 4 and 5 are 10.6 and 3.2 A. The results show:

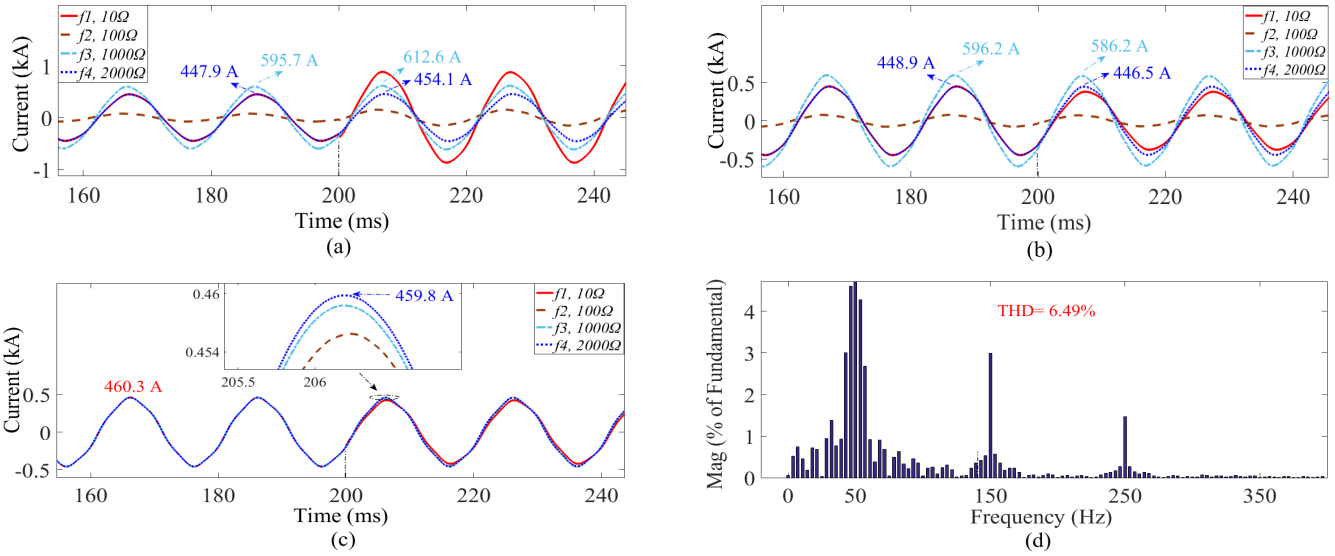

FIGURE 11. FPCs on each feeder under different fault cases. (a) FFU. (b) FFD. (c) Normal feeder $F_{(2)}$. (d) FFT to FPC-on-FFD.

TABLE 5. Results of faulty phase detection under different fault cases.

Case	*Fault position*	Z_f (Ω)	Δ_U (V)			Δ_θ (°)			$\Delta_U \cdot \Delta_\theta$			*Faulty phase*
			A	B	C	A	B	C	A	B	C	
1	f_5	0.1	-666.4	101.2	182	\	\	\	\	\	\	A
2	f_2	5	-609.2	55.1	-219.2	-3.41	-1.08	3.60	+	-	-	A
3	f_3	50	-144.8	27.0	86.9	\	\	\	\	\	\	A
4	f_4	500	-25.1	-10.2	6.3	1.81	-0.73	1.36	-	+	+	A
5	f_5	1500	-6.1	-2.6	4.4	0.67	-0.32	0.72	-	+	+	A

1) The Δ_U of faulty phase A in all cases are negative (marked in bule), which is consistent with (3).
2) There are one dropped and two raised voltages in Case 1 and 3 (K_u in Area 3). According to Step 1 in Fig. 5, the only dropped-voltage phase A is detected as the faulty phase.
3) There are one raised and two dropped voltages in Case 2, 4, and 5 (K_u in Area 1 or 2). At this time, it is necessary to further calculate the Δ_θ and multiply it with the corresponding Δ_U. According to Step 1 in Fig. 5, the phase A with unique $\Delta_U \cdot \Delta_\theta$ among three phases is detected as the faulty phase. For example, there are $\Delta_U \cdot \Delta_\theta > 0$ for the phase A and $\Delta_U \cdot \Delta_\theta < 0$ for phases B and C in Case 2.
4) In Case 5, even if Z_f is 1500 Ω, the $\Delta_U \cdot \Delta_\theta$ of faulty phase A is still unique among three phases, which does not change the effectiveness of faulty phase detection.

After the faulty phase is detected, Table 4 shows the Δ_I and faulty feeder detection results under these cases. The results show:

1) In all cases, there are $\Delta_I > 0$ for faulty feeders (marked in bule). The $F_{(5)}$ in Case 3 is a branch of $F_{(6)}$ (see Fig. 6), so there is $\Delta_I > 0$ for $F_{(5)}$. On the contrary, there are $\Delta_I < 0$ for normal feeders. They are consistent with (11) and (15).
2) According to Step 2 in Fig. 5, the feeder with $\Delta_I > 0$ is detected as the faulty feeder. For example, the Δ_I of $F_{(2)}$ is 405.2 A, and there are $\Delta_I < 0$ for other feeders in Case 1.
3) In Case 5, even if Z_f is 1500 Ω, there are still $\Delta_I > 0$ for the faulty feeder $F_{(2)}$ and $\Delta_I < 0$ for other feeders, which does not change the effectiveness of faulty feeder detection.

After the faulty feeder is detected, Table 7 shows the Δ_I of CTs on faulty feeders and the fault section detection results. The values of CTs in Table 7 are the Δ_I of faulty feeders in Table 6. $CT_1 - CT_7$ correspond to each position in Fig. 6, and \ means that this CT is not needed. The results show:

1) In all cases, there are $\Delta_I > 0$ for FFU (marked in bule) and $\Delta_I < 0$ for FFD, which is consistent with (11) and (13). In Case 1, for example, CT and CT_5 are on FFU, and their Δ_I are 405.2 and 405.4 A; while CT_7 is on FFD, and its Δ_I is −387.9 A.
2) According to Step 3 in Fig. 5, the section $[CT_i, CT_{i+1}]$ with the following feature is detected as the faulty section: $\Delta_I > 0$ for CT_i and $\Delta_I < 0$ for CT_{i+1}.

TABLE 6. Results of faulty feeder detection under different fault cases.

Case	Fault position	Z_f (Ω)	Δ_I (A) on feeders								Faulty feeder
			$F_{(1)}$	$F_{(2)}$	$F_{(3)}$	$F_{(4)}$	$F_{(5)}$	$F_{(6)}$	$F_{(7)}$	$F_{(8)}$	
1	f_5	0.1	-35.4	405.2	-5.0	-2.9	-5.5	-51.9	-7.6	-8.5	$F_{(2)}$
2	f_2	5	-68.0	-40.0	-10.4	-5.1	-11.0	-105.1	580.0	-17.7	$F_{(7)}$
3	f_3	50	-6.0	-5.1	-1.0	-0.5	85.0	48.4	-1.6	-1.8	$F_{(5)}$
4	f_4	500	35.7	-3.0	-0.3	-0.2	-0.7	-7.1	-1.1	-1.3	$F_{(1)}$
5	f_5	1500	-0.59	7.65	-0.08	-0.04	-0.09	-0.87	-0.12	-0.14	$F_{(2)}$

3) In Case 5, even if Z_f is 1500 Ω, the Δ_I on FFU is 7.65 A, and the Δ_I on FFD is −1.07 A, which does not change the effectiveness of faulty section detection.
4) Although Case 3 is a fault on the feeder branch, as long as a CT is installed on the branch, no matter how complex the branch is, the fault on the branch can be located.

D. FURTHER ROBUSTNESS TESTS

Nowadays, to save electricity costs and improve energy efficiency, more and more DGs are connected to the grid, which makes distribution networks more complex. Also, the damping of network varies with weathers. They make the power quality problems such as harmonics (noise) and three-phase imbalance serious, so it is necessary to test the robustness of proposed method under these conditions.

We close S_1 and S_2 in Fig. 6, connect DG_1 and DG_2 to the network, and let them generate harmonics and unbalanced voltages. Also, considering countries with long feeders, such as Australia, we set the length of feeders $F_{(1)} - F_{(8)}$ as 50-100 km. When the phase A is grounded by 10 Ω at f_4, the bus voltages and FPCs on feeders are shown in Fig. 12(a) and (b), and the pre-fault and post-fault amplitudes have been marked. The FFT to FPC-on-$F_{(3)}$ is shown in Fig. 12(c). At this time, the DG_1 is on FFU and DG_2 is on the normal feeder. The results show:

1) In Fig. 12(a), even if the three-phase imbalance and harmonics exceed the limit seriously (THD is 21.6% in Fig. 12(c)), there are one dropped FPV and two raised NPVs under the fault, and the proposed method can still detect the faulty phase.
2) In Fig. 12 (b), the FPC on FFU rises, while the FPCs on FFD and normal feeders drop. The proposed method can still detect the faulty section.
3) The fastest execution time of proposed method is only two post-fault cycles (40 ms). The first cycle is the transient cycle without sampling, and the second cycle is the steady-state cycle with sampling.
4) The fundamental reason why the proposed method is effective under the environments is that it extracts the (voltage and current) amplitude differences between the pre-fault and post-fault. For the same phase or feeder, the three-phase imbalance exists before and after faults, and can be regarded as a constant within the execution time of its MS-level algorithm. Therefore, its impact on the method has been automatically eliminated by Δ, see (6), (7), and (9). Also, the extracted bus voltages and FPCs are periodic signals in the steady state. From the Fourier series, we can see that they already contain various harmonics, that is, the impact of harmonics has been taken into account by the method. Therefore, this method is robust under three-phase imbalance and harmonics.

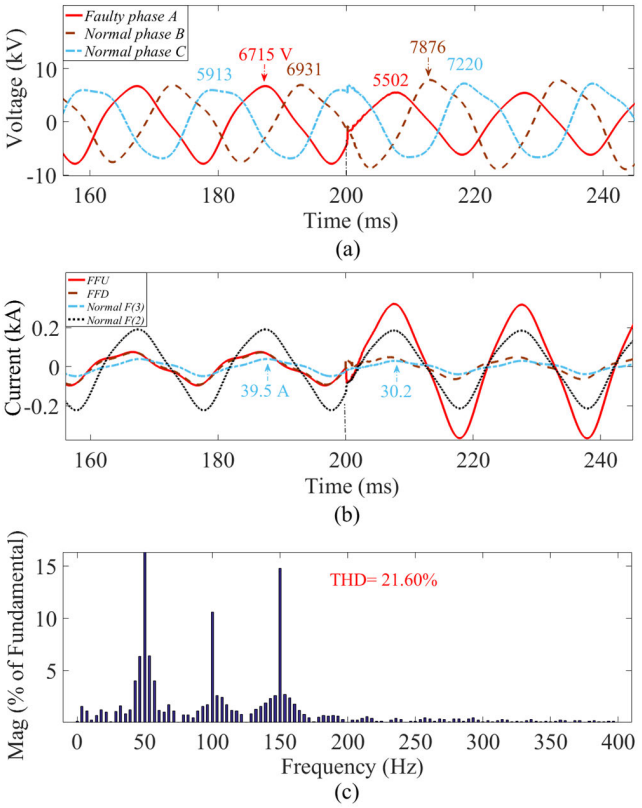

FIGURE 12. Tests under harmonics and three-phase imbalance. (a) Bus voltages. (b) FPCs on feeders. (c) FFT to FPC-on-$F_{(3)}$.

We connect S_1 and disconnect S_2 to test the proposed method. The bus voltages and FPCs on feeders are shown in Fig. 13(a) and (b) when the phase A is grounded by 10 Ω at f_1. At this time, only DG_1 is connected to the network and is on FFD. The results show:

1) In Fig. 13(a), the FPV drops and NPVs rise. For FPCs in Fig 13(b), the FFU rises and the DFF and normal

TABLE 7. Results of faulty section detection under different fault cases.

Case	*Fault position*	Z_f (Ω)	Δ_I (A) *on faulty feeder*								*Faulty section*
			CT	CT_1	CT_2	CT_3	CT_4	CT_5	CT_6	CT_7	
1	f_5	0.1	405.2	\	\	\	\	405.4	\	-387.9	CT_5-CT_7
2	f_2	5	580.0	\	-36.5	\	\	\	-36.5	\	CT -CT_2
3	f_3	50	85.0	\	\	-6.2	\	\	\	\	CT -CT_3
4	f_4	500	35.7	36.7	\	\	-4.2	\	\	\	CT_1-CT_4
5	f_5	1500	7.65	\	\	\	\	7.65	\	-1.07	CT_5-CT_7

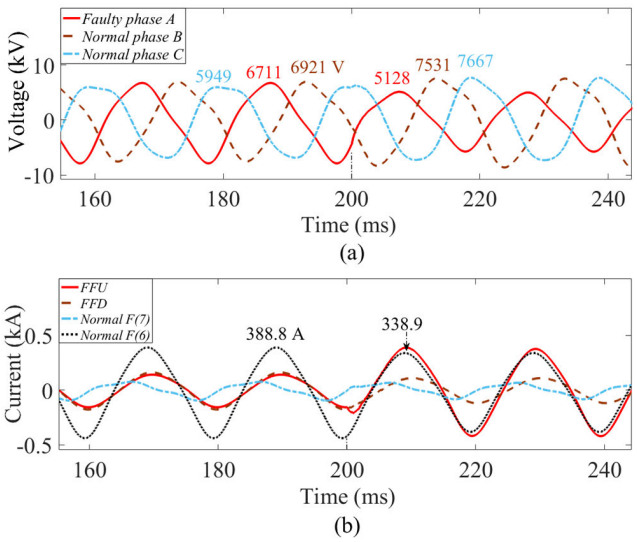

FIGURE 13. Tests under different network topologies. (a) Bus voltages. (b) FPCs on feeders.

feeders drop. Combined with Fig. 12, we can conclude that the proposed method is effective no matter where the DGs are. This is because the capacities of DGs are limited (in China's distribution networks, the capacity of a DG does not exceed 30% of that of SG), which is far less than the sum of the capacities of SG and other DGs, making the total power flow direction of feeders is still consistent with that of single-source radiation networks.

2) Even if the feeder lengths in model are 50-100 km, the proposed method is still effective.

E. COMPARISON WITH EXISTING METHODS

In recent years, there are many ZSC-based fault detection methods such as [2] and [3], but we have to admit that the ZSC is extremely weak under high impedance faults, and it is difficult to extract. Fig. 14(a) and (b) show the FPCs and ZSCs on faulty and normal feeders when Z_f is 1500 Ω. The results show that the ZSCs on faulty and normal feeders are only 2.1 and 0.6 A. Also, there are natural ZSCs caused by unbalanced lines and loads, which makes it more difficult to extract the ZSC under SLG faults. On the contrary, the proposed method only needs to extract the bus voltages and feeder FPCs, and their values are high even under high impedance faults, which is easy to extract by CTs. In Fig. 14, for example, the pre-fault and post-fault FPCs on the faulty feeder are 579.5 and 588.5 A, and Δ_{Iu} is 9 A; the pre-fault and post-fault FPCs on the normal feeder are 80 and 78.3 A, and Δ_{In} is -1.7 A. Both $|\Delta_{Iu}|$ and $|\Delta_{In}|$ are also higher than the corresponding ZSCs. Therefore, the proposed method is more robust than ZSC-based methods under high impedance faults.

Compared with some smart methods based on signal processing such as [8] and [9], the proposed method only needs to extract the pre-fault and post-fault bus voltages and feeder currents without signal conversion, and has a simple algorithm, which is easy to implement in engineering.

Compared with some faulty feeder detection methods such as [17] and [18], the proposed method can further locate faults.

Compared with some methods based on smart devices, such as [21] and [22], the proposed method only needs to monitor bus voltages and feeder currents. The bus voltage monitoring has been realized in distribution networks, and the

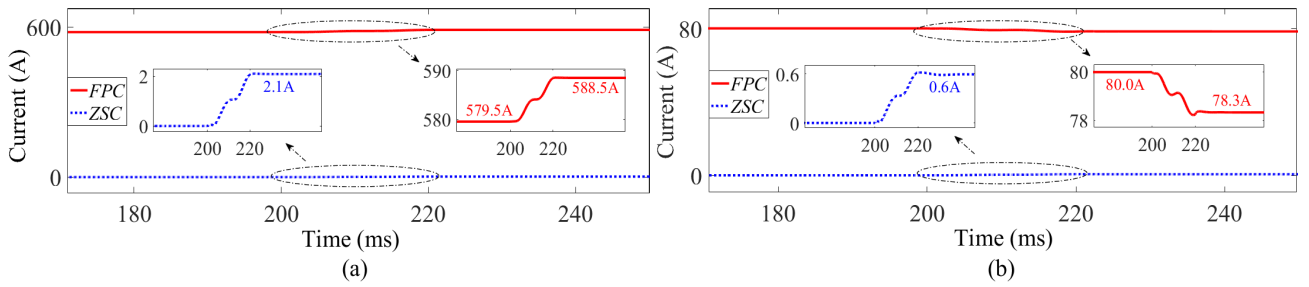

FIGURE 14. Amplitudes of FPCs and ZSCs under Z_f is 1500 Ω. (a) Faulty feeder. (b) Normal feeder.

feeder current monitoring only needs common low-cost CTs. Therefore, this method is quite friendly to non-developed countries and regions.

In particular, references [26] and [29] obtained the Voltage-Current characteristic on transmission lines by the PMUs and digital image processing method, so as to locate the faults in transmission networks. Compared with them, the proposed method can locate the faults only by subtractions and plus-minus sign comparisons using lower-cost transformers, so the proposed method in this paper is simpler.

V. CONCLUSION

In this paper, the following SLG features in RGS are obtained by analyzing the fault distortions of bus voltages and feeder FPCs. 1) The bus voltages have one of the following distortions. One dropped FPV and two raised NPVs. One dropped FPV and two NPVs (in which one rises and the other drops), where the product of FPV amplitude distortion and its phase-angle distortion is unique among three phase voltages. 2) The FPC on FFU rises, while the FPCs on FFD and normal feeders drop.

Moreover, the VFA K_u and FDs Δ are defined to quantify the above-mentioned fault features, and a fault location method based on FDs is proposed. It can be simply implemented by the pre-fault and post-fault bus voltages and feeder FPCs. Simulation tests show that the proposed method is robust under high impedance faults, harmonics, and three-phase imbalance.

In future research, the proposed method will be extended to the transmission networks and other neutral distribution networks such as ungrounded and resistance grounded neutrals.

APPENDIX

For Fig. 4, the Node Admittance Equation is established with reference to the node **0**:

$$\left(3Y_{eq}+Y_f+Y_p\right)V_1-\left(Y_{eq}+Y_f\right)E_a-Y_{eq}E_b-Y_{eq}E_c=0 \tag{A-1}$$

where V_1 is the potential of load grounded node **1**.

Solving for (A-1), V_1 is

$$V_1=\frac{Y_f}{3Y_{eq}+Y_f+Y_p}E_a \tag{A-2}$$

Therefore, The FPCs on FFU, FFD, and normal feeders are

$$I_u=(E_a-V_1)\left(Y_{eq(n)}+Y_f\right) \tag{A-3}$$

$$I_d=(E_a-V_1)Y_{eq(n)} \tag{A-4}$$

$$I_n=(E_a-V_1)Y_{eq(j)} \tag{A-5}$$

Finally, we can get (10), (12), and (14) from (A-2) - (A-5).

REFERENCES

[1] X. Wang, J. Gao, X. Wei, Z. Zeng, Y. Wei, and M. Kheshti, "Single line to ground fault detection in a non-effectively grounded distribution network," *IEEE Trans. Power Del.*, vol. 33, no. 6, pp. 3173–3186, Dec. 2018.

[2] P. Wang, H. Zhou, B. Chen, C. Tian, B. Chen, and B. Sun, "Fault location method in resonant grounded networks based on distributed modulation and compensation adjustment," *IEEE Trans. Power Del.*, vol. 34, no. 5, pp. 1938–1947, Oct. 2019.

[3] X. Wang, H. Zhang, F. Shi, Q. Wu, V. Terzija, W. Xie, and C. Fang, "Location of single phase to ground faults in distribution networks based on synchronous transients energy analysis," *IEEE Trans. Smart Grid*, vol. 11, no. 1, pp. 774–785, Jan. 2020.

[4] P. Liu and C. Huang, "Detecting single-phase-to-ground fault event and identifying faulty feeder in neutral ineffectively grounded distribution system," *IEEE Trans. Power Del.*, vol. 33, no. 5, pp. 2265–2273, Oct. 2018.

[5] M. A. Barik, A. Gargoom, M. A. Mahmud, M. E. Haque, H. Al-Khalidi, and A. M. Than Oo, "A decentralized fault detection technique for detecting single phase to ground faults in power distribution systems with resonant grounding," *IEEE Trans. Power Del.*, vol. 33, no. 5, pp. 2462–2473, Oct. 2018.

[6] Y. Wang, Y. Huang, X. Zeng, G. Wei, J. Zhou, T. Fang, and H. Chen, "Faulty feeder detection of single phase-Earth fault using grey relation degree in resonant grounding system," *IEEE Trans. Power Del.*, vol. 32, no. 1, pp. 55–61, Feb. 2017.

[7] Y. Li, X. Yin, and R. Chen, "New method for transient line selection in distribution system based on grounding fault transferred," *J. Eng.*, vol. 2019, no. 16, pp. 2822–2826, Nov. 2018.

[8] J. Shangbin, G. Jingwen, L. Yunjun, and X. Ting, "A novel single-phase-to-Earth fault line method in small current grounding systems," in *Proc. Chin. Control Conf. (CCC)*, Jul. 2019, pp. 7310–7315.

[9] X. J. Zeng, K. Yu, Y. Wang, and Y. Xu, "A novel single phase grounding fault protection scheme without threshold setting for neutral ineffectively Earthed power systems," *CSEE J. Power Eng. Syst.*, vol. 2, no. 3, pp. 73–81, Sep. 2016.

[10] M.-F. Guo, X.-D. Zeng, D.-Y. Chen, and N.-C. Yang, "Deep-learning-based Earth fault detection using continuous wavelet transform and convolutional neural network in resonant grounding distribution systems," *IEEE Sensors J.*, vol. 18, no. 3, pp. 1291–1300, Feb. 2018.

[11] H. Hasanvand, A. Parastar, B. Arshadi, M. R. Zamani, and A. S. Bordbar, "A comparison between S-transform and CWT for fault location in combined overhead line and cable distribution networks," in *Proc. 21st Conf. Electr. Power Distrib. Netw. Conf. (EPDC)*, Apr. 2016, pp. 266–271.

[12] Z. Guo, J. Yao, and Z. Tan, "Hilbert–Huang transform–based transient busbar protection algorithm," *IET Gener., Transmiss. Distrib.*, vol. 9, no. 14, pp. 2032–2039, Nov. 2015.

[13] A. Gururani, S. R. Mohanty, and J. C. Mohanta, "Microgrid protection using Hilbert–Huang transform based-differential scheme," *IET Gener., Transmiss. Distrib.*, vol. 10, no. 15, pp. 3707–3716, Nov. 2016.

[14] Z. Zhang, M. Wang, Y. Xiang, and A. Nehorai, "Geometry-adapted Gaussian random field regression," in *Proc. IEEE Int. Conf. Acoust., Speech Signal Process. (ICASSP)*, Mar. 2017, pp. 6528–6532.

[15] E. Chevallier and J. Angulo, "Image adapted total ordering for mathematical morphology on multivariate images," in *Proc. IEEE Int. Conf. Image Process. (ICIP)*, Oct. 2014, pp. 2943–2947.

[16] M. A. Barik, A. Gargoom, M. A. Mahmud, M. E. Haque, A. M. T. Oo, and H. Al-Khalidi, "Mathematical morphology-based fault detection technique for power distribution systems subjected to resonant grounding," in *Proc. IEEE Power Energy Soc. Gen. Meeting*, Jul. 2017, pp. 178–183.

[17] L. Shilong, T. Yufei, L. Xiaopeng, Z. Huajie, and F. Shilin, "Fault line selection of single phase grounding fault in small-current ground system based on reactive current," in *Proc. IEEE Innov. Smart Grid Technol. Asia (ISGT Asia)*, May 2019, pp. 138–143.

[18] X. Z. Dong, J. Wang, S. Shi, B. Wang, B. Dominik, and M. Redefern, "Traveling Wave based single-phase-to-ground protection method for power distribution system," *CSEE J. Power Eng. Syst.*, vol. 1, no. 2, pp. 75–81, Jun. 2015.

[19] B. Liu, H. Ma, H. Xu, and P. Ju, "Single-phase-to-ground fault detection with distributed parameters analysis in non-direct grounded systems," *CSEE J. Power Eng. Syst.*, vol. 5, no. 1, pp. 139–147, Mar. 2019.

[20] Z. Cong, Y. Liu, J. Fang, P. Wang, L. Guo, and X. Jiang, "Root-cause identification of single line-to-ground fault in urban small current grounding systems based on correlation dimension and average resistance," *IEEE Trans. Power Del.*, vol. 35, no. 4, pp. 1834–1843, Aug. 2020, doi: 10.1109/TPWRD.2019.2955185.

[21] Y. Jiang, "Data-driven fault location of electric power distribution systems with distributed generation," *IEEE Trans. Smart Grid*, vol. 11, no. 1, pp. 129–137, Jan. 2020.

[22] J.-H. Teng, W.-H. Huang, and S.-W. Luan, "Automatic and fast faulted line-section location method for distribution systems based on fault indicators," *IEEE Trans. Power Syst.*, vol. 29, no. 4, pp. 1653–1662, Jul. 2014.
[23] K. Jia, Z. Ren, T. Bi, and Q. Yang, "Ground fault location using the low-voltage-side recorded data in distribution systems," *IEEE Trans. Ind. Appl.*, vol. 51, no. 6, pp. 4994–5001, Nov. 2015.
[24] A. Tashakkori, P. J. Wolfs, S. Islam, and A. Abu-Siada, "Fault location on radial distribution networks via distributed synchronized traveling wave detectors," *IEEE Trans. Power Del.*, vol. 35, no. 3, pp. 1553–1562, Jun. 2020.
[25] D. P. Kothari and I. J. Nagrath, *Modern Power System Analysis*, 4th ed. New Delhi, India: Tata, 2011, pp. 124–135.
[26] A. Abu-Siada, M. I. Mosaad, and S. Mir, "Voltage–current technique to identify fault location within long transmission lines," *IET Gener., Transmiss. Distrib.*, vol. 14, no. 23, pp. 5588–5596, Dec. 2020.
[27] J. Yin, Y. Chen, and Z. Li, "Research on line selection of single-phase grounding fault in neutral ungrounded system based on phase current distortion," in *Proc. 9th Int. Conf. Power Energy Syst. (ICPES)*, Dec. 2019, pp. 1–6.
[28] Y. D. Xue, J. Li, X. Chen, B. Xu, and T. Li, "Faulty feeder selection and transition resistance identification of high impedance fault in a resonant grounding system using transient signals," *Chin. Soc. Elec. Eng.*, vol. 37, no. 17, pp. 5037–5048, Sep. 2017.
[29] A. Abu-Siada and S. Mir, "A new on-line technique to identify fault location within long transmission lines," *Eng. Failure Anal.*, vol. 105, pp. 52–64, Nov. 2019.

YOUGEN CHEN received the Ph.D. degree in electrical engineering from the University of Tsukuba, Japan, in 2009. He is currently an Associate Professor with the School of Automation, Central South University, China. His research interests include power system planning, multiple criteria decision-making, and power electronics control in distributed generation fields.

JUNBO YIN received the B.S. degree from the Hunan Institute of Engineering, China, in 2018. He is currently pursuing the M.S. degree in electrical engineering with Central South University, China. His research interests include power system fault detections and power quality control.

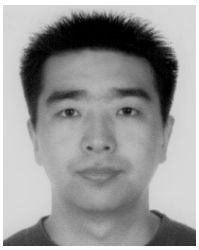

ZHIYONG LI received the Ph.D. degree from Central South University, China, in 2006. From 2007 to 2008, he was a Visiting Scholar with the Power System Laboratory, Swiss Federal Institute of Technology. He is currently an Associate Professor with the School of Automation, Central South University. His research interests include power system fault prediction and multi-objective optimization in distribution networks.

RENYONG WEI received the B.S. degree from Zhejiang University, in 1984, and the M.S. degree from Southwest Jiaotong University, in 1987. He is currently a Professor with the School of Automation, Central South University, China. His research interests include power system modeling, reliability assessment, and power quality optimization.